

# CO<sub>2</sub> Top-of-the-Line Corrosion in Presence of Acetic Acid: A Parametric Study

M. Singer,<sup>‡</sup>\* D. Hinkson,\* Z. Zhang,\* H. Wang,\* and S. Nešić\*

## ABSTRACT

*This research presents the results of an experimental study, performed in a flow loop, of five parameters identified as having a significant influence on top-of-the-line corrosion (TLC): partial pressure of carbon dioxide (CO<sub>2</sub>), condensation rate, gas temperature, organic acid concentration, and gas velocity. A comprehensive analysis of the effect of each of these five parameters on the type of corrosion is performed. Experimental data related to uniform corrosion, pitting, and mesa attack are presented and provide an inclusive view of the phenomena involved in TLC in sweet environments. It is proposed that the relatively small volume of the droplet can become supersaturated with respect to iron carbonate (FeCO<sub>3</sub>), as a result of the initially high average corrosion rate. Depending on the conditions, the precipitation of FeCO<sub>3</sub> on the metal surface can decrease significantly the average corrosion rate. However, the protectiveness of this layer is challenged by the rate of droplet renewal (water condensation rate) and the overall corrosivity of the environment (CO<sub>2</sub> content, acetic acid concentration). Very aggressive localized corrosion can be initiated and sustained. The extent of TLC is definitively the result of complex interactions between all of these parameters. Threshold values, often used as engineering guidelines in the industry, should be used with caution, and a solid understanding of the mechanisms involved is a prerequisite for the development of effective TLC inhibition program.*

**KEY WORDS:** acetic acid, CO<sub>2</sub> corrosion, condensation, top-of-the-line corrosion

Submitted for publication: May 10, 2012. Revised and accepted: January 16, 2013. Preprint available online: February 5, 2013. <http://dx.doi.org/10.5006/0737>.

<sup>‡</sup> Corresponding author. E-mail: [singer@ohio.edu](mailto:singer@ohio.edu).

\* Institute for Corrosion and Multiphase Technology, Ohio University, 342 West State St., Athens, OH 45701.

## INTRODUCTION

The transportation of fluids in pipelines is a critical step in oil and gas production. When it comes directly from the well, the fluid is unprocessed, multiphase, and can be a mixture of oil, solids, gas, and water. The presence of water leads to considerable corrosion problems on the internal walls of the pipelines. The phenomenon of interest in this study is the transportation of wet gas and, more precisely, the top-of-the-line corrosion (TLC) that occurs when significant heat exchange is present between the pipelines and the surroundings (frozen land, seawater). The unprocessed vapor flowing through the pipe condenses on the cold walls, forming a thin film and/or droplets of liquid. The liquid can contain corrosive species such as organic acids and dissolved corrosive gases (such as carbon dioxide or hydrogen sulfide). Therefore, the condensation of wet gas can lead to a very corrosive environment. The first case of TLC observed in the field was reported in the 1960s in a sour gas field in France.<sup>1</sup> Since then, numerous cases have been reported, mostly offshore<sup>2-6</sup> but also on several occasions onshore.<sup>7-8</sup> As it is reported, TLC occurs exclusively in stratified flow regimes, at low gas velocity, and in sweet or sour environments. The condensation rate and the presence of organic acid seem to be controlling parameters.

The objective of this work was to conduct an experimental study covering some of the main parameters influencing TLC, namely, the water condensation rate, the partial pressure of CO<sub>2</sub>, the gas temperature, the acetic acid concentration, and the gas velocity.

ity. The goal was to better understand the influence of each of these parameters on the TLC mechanism. The study was performed in a large-scale flow loop under realistic flowing conditions, and the corrosion rates (general and localized) were measured using weight-loss samples made of pipeline steel.

## REVIEW OF PREVIOUS WORK

In the past 20 years, TLC has been the subject of intensive research. Olsen and Dugstad<sup>9</sup> conducted a systematic experimental study on parameters influencing TLC in sweet conditions. The formation of a protective iron carbonate ( $\text{FeCO}_3$ ) corrosion product layer was suggested to play a key role:



The precipitation of  $\text{FeCO}_3$  only occurs when the saturation level is above unity as defined below:

$$\text{Saturation}_{\text{FeCO}_3} = \frac{[\text{CO}_3^{2-}] \times [\text{Fe}^{2+}]}{K_{\text{sp}}} \quad (2)$$

with  $K_{\text{sp}}$ : solubility product of  $\text{FeCO}_3$

High levels of super-saturation (saturation of  $\text{FeCO}_3$  above unity) could lead to very dense and protective  $\text{FeCO}_3$ , as it was experienced at a high temperature (70°C) and a low condensation rate. The authors also found that the competition between  $\text{FeCO}_3$  film formation kinetics and the condensation rates controlled the extent of the corrosion attack. At a high condensation rate, the saturation in  $\text{FeCO}_3$  is more difficult to obtain because of the rate of fresh water renewal. DeWaard, et al.,<sup>10</sup> proposed the first modeling approach to TLC based on his famous full pipe flow empirical equation.

In 1999, Gunaltun and Larrey<sup>5</sup> added more insight into TLC mechanisms by defining three main zones in the pipeline:

- The bottom of the pipe where the corrosion can be lowered with the use of inhibitors.
- At the sidewall of the pipe where the condensed water drains to the bottom. The corrosion is uniform but inhibitors are not efficient.
- At the top of the line where a protective iron carbonate layer can be formed in certain cases. Inhibitors are not effective and localized corrosion occurs.

The condensation rate was identified once again as a controlling parameter in TLC and the concept of critical condensation rate grew stronger. It was set at 0.25 mL/m<sup>2</sup>/s with values being calculated considering that all the water vapor condenses on half of the pipe only. If large quantities of organic acid are present, this critical threshold is reduced to 0.025 mL/m<sup>2</sup>/s.<sup>11</sup>

In 2000, a new model was proposed by Pots and Hendriksen,<sup>12</sup> which strived at taking into account the competition between the scale formation rate linked to the iron dissolution and the condensation rate. The so-called “super saturation model” is based on the calculation of the concentration of iron at saturation under film-forming conditions. Pots and Hendriksen<sup>12</sup> insisted on the importance of correctly evaluating the condensation rate to predict accurately the corrosion rate.

In 2002, Vitse and coworkers<sup>13-15</sup> completed a thorough experimental and theoretical study on TLC caused by carbon dioxide ( $\text{CO}_2$ ). Condensation and corrosion experiments were conducted in a large-scale, 4 in (0.1 m) inner diameter (ID) flow loop. Vitse developed two models and adapted them to a top-of-the-line scenario: a mechanistic film-wise condensation model based on Nusselt theory and a semi-empirical corrosion model. The condensation model has a sound mechanistic approach and is based on the assumption that a continuous film of liquid covers the steel surface at the top of the line (filmwise condensation). Vitse acknowledges that, while this approach is valid in estimating the condensation rate on the side of the pipe, it is not ideal to cover the condensation process happening at the top (11 to 1 o'clock positions) which is drop-wise.<sup>5</sup> Nevertheless, Vitse's corrosion model constituted a considerable breakthrough in the understanding of the mechanisms involved in TLC.

Between 2002 and 2007, several experimental studies<sup>16-17</sup> were published on the effect of different parameters such as acetic acid, MEG, or pH control. The presence of acetic acid was known to greatly affect TLC in particular and mild steel corrosion in general.<sup>18</sup>

Strong advances in TLC research were published in 2007. A series of papers presented additional experimental work and guidelines for field operation.<sup>19-21</sup> The same year, Zhang, et al.,<sup>22</sup> published the first fully mechanistic approach in TLC modeling, covering the three main processes involved in top-of-the-line corrosion phenomena:

- dropwise condensation
- chemistry in the condensed water
- corrosion at the steel surface

Most of the experimental data presented in the current study compare well to Zhang's model, as reported elsewhere.<sup>22</sup> Zhang's approach represents one of the most advanced attempts to model the mechanisms involved in TLC to date. It takes into account the most important parameters in  $\text{CO}_2$  TLC:

- condensation rate
- gas temperature
- $\text{CO}_2$  partial pressure
- gas velocity
- acetic acid concentration

Since then, experimental studies have been published on  $\text{H}_2\text{S}$  TLC,<sup>23-24</sup> on the characteristics of the

water condensation at the top of the line,<sup>25</sup> and on the possible role of hydrocarbon condensate.<sup>4</sup> Remita, et al.,<sup>26</sup> built upon the work proposed by Vitse, et al.,<sup>13</sup> and developed a model for CO<sub>2</sub> corrosion under thin liquid film.

Even though much progress has been made over the years on the understanding of TLC mechanisms, none of the models proposed thus far tackles the occurrence and prediction of localized corrosion. The first experimental study focusing on this aspect linked to the TLC phenomena was published by Amri, et al.,<sup>27</sup> in an effort to relate pit growth and environmental conditions. A conceptual model of pit propagation and growth was proposed, although more validation work clearly is needed.

The present work presents a systematic experimental study of the main parameters influencing TLC performed in realistic flow loop conditions. Important information about average and localized corrosion were collected, and the data have been used to validate and improve the current understanding of the mechanism.

## EXPERIMENTAL PROCEDURES

A useful approach toward understanding any mechanism is to select a baseline condition and to vary one parameter at a time. That is what has been done throughout the work presented here. In addition, some tests have focused on the study of interacting effects between parameters. This approach provides better insight into the relative weight of each parameter and helps in identifying specific areas of interest where the current understanding remains limited.

The most important five parameters were identified as follows:

- gas velocity
- undissociated acetic acid concentration
- condensation rate
- CO<sub>2</sub> partial pressure
- gas temperature

One interacting effect was investigated:

- condensation rate/acetic acid

Table 1 presents the experimental conditions of the baseline test. Each series of tests proposes a vari-

**TABLE 1**  
*Baseline Conditions*

Parameters	Baseline Conditions
<i>Absolute pressure (bar)</i>	3
<i>pCO<sub>2</sub> (bar)</i>	2
<i>Gas temperature (°C)</i>	70
<i>Condensation rate (mL/m<sup>2</sup>/s)</i>	0.25
<i>Gas velocity (m/s)</i>	5
<i>pH<sub>2</sub>S (bar)</i>	0
<i>Free HAc concentration in the tank (mg/L)</i>	0
Steel type	API X65
Liquid phase composition	DI water
pH (tank)	4.5
Test duration (weeks)	3

Only the value of the parameters in italic will be varied on this study.

ation of a single parameter around the baseline conditions. Table 2 shows the range of values in which each parameter is varied. Some liquid accumulated at the bottom of the line as a result of the water condensation forming a small liquid stream. The flow regime could be observed through a high-pressure transparent window and always was clearly stratified.

Another important aspect is the wall temperature at the top of the line, where the corrosion reaction takes place. This wall temperature is dependent on the gas temperature, the condensation rate, and, to a lesser extent, the total pressure and the gas velocity. The corresponding values encountered in this experimental study are shown in Table 3. These values are calculated using an approach developed by Zhang, et al.,<sup>22</sup> which shows very good agreement with experimental measurements.

### Large-Scale Loop

Experiments were carried out in two similar high-temperature, high-pressure, 4 in ID flow loops. The liquid tank, gas blower, and pipes represent a 30 m long system made of stainless steel. Specially designed test sections enabled the insertion of cylindrical weight-loss coupons made of carbon steel. The test section is shown in Figure 1. The main liquid phase in the tank is heated to the required temperature using immersion heaters. The vapor phase containing water and acetic acid vapors, CO<sub>2</sub> and N<sub>2</sub> gases is circulated through the pipe system while no

**TABLE 2**  
*Range of Variables*

Parameters	Range		
	Min	Medium	Max
Absolute pressure (bar)	3	3	8
pCO <sub>2</sub> (bar)	0.13	2	8
Gas temperature (°C)	40	70	90
Condensation rate (mL/m <sup>2</sup> /s)	0.05	0.25	1
Gas velocity (m/s)	5	10	15
Free HAc concentration in the tank (mg/L)	0	100	1,000

NB: The absolute pressure is not varied independently of the CO<sub>2</sub> partial pressure

**TABLE 3**  
Wall Temperature

Gas Temperature (°C)	Condensation Rate (mL/m <sup>2</sup> /s)	Total Pressure (bar)	Wall Temperature (°C)
70	0.03	3	69.8
70	0.25	3	68.2
70	1	3	63.2
40	0.25	3	33.5
70	0.25	0.13	68.3
70	0.25	8.3	67.8

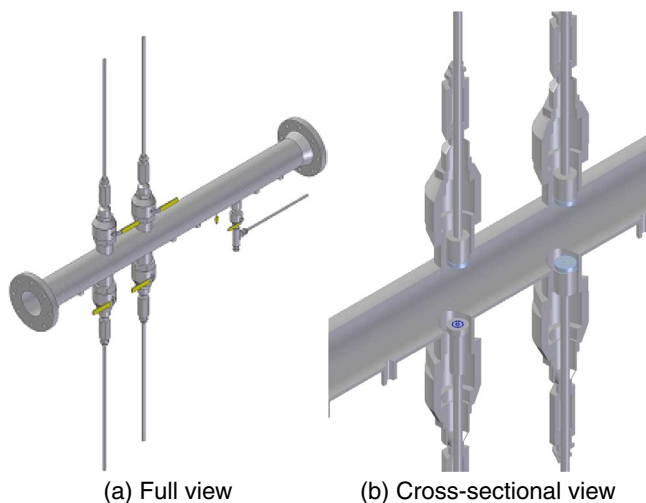


**FIGURE 1.** Typical TLC test section.

liquid from the tank is carried (only the gas phase is circulated). A more detailed description of one of the flow loops and its equipment was presented by Singer, et al.,<sup>16</sup> in 2004.

### Water Condensation Rate

The condensation conditions were simulated using cooling coils wrapped around the pipe. The condensation rate was measured by collecting the condensed water downstream of the test section. The present study was performed in an environment made of CO<sub>2</sub> and water. In actual pipelines, it is fully expected that light hydrocarbons will co-condense together with the water vapor. Water/oil wetting at the top of the line is indeed an important parameter to consider. Recent work seems to show that the hydrophilic nature of the steel favors water-wetting<sup>27</sup> but the water/hydrocarbon condensation-rate ratio must also play a key role and should be studied further.

### Liquid Phase Composition

The liquid phase is made up exclusively of deionized water; no salt is added. However, dissolved ferrous iron, Fe<sup>2+</sup>, buildup occurs throughout the test as a result of the corrosion process on the weight-loss coupons. pH was monitored regularly in the main liquid storage tank and liquid samples also were taken.

Although the pH in the main tank did vary between tests from 3.5 to 4.8 depending on the conditions, there was no direct influence on the liquid composition at the top of the line, which was always pure condensed water. In fact, the pH in the main tank had to be considered only when evaluating the concentration of free acetic acid.

### Scale Formation

There is no easy way to measure the evolution of the pH in the condensed water at the top of the line. The fresh condensed liquid has a relatively low pH, because it is pure water saturated with CO<sub>2</sub>. Calculations have shown that the pH can be initially as low as 3.2 to 4. However, as the corrosion process starts, the iron concentration in the condensed droplet rises quickly. Depending on the condensation rate and on the droplet size, conditions for FeCO<sub>3</sub> saturation also can be met more or less rapidly inside the droplet.

### Acetic Acid Concentration

The acetic acid (HAc) concentration is adjusted by adding a calculated amount of deoxygenated pure HAc in the tank. The acid then dissociates to form acetate (Ac<sup>-</sup>) and hydrogen ions (H<sup>+</sup>). The remaining amount of free acetic acid (which depends on the pH) defines the concentration of total acetic acid present in the condensed liquid at the top of the line. A comprehensive study on the thermodynamics of water/HAc/liquid vapor equilibrium was published by Hinkson, et al.,<sup>25</sup> in 2007. This study shows that, in the range of parameters tested in the present study, the concentration of total acetate species in the condensed water should be very similar to or slightly lower than the concentration of undissociated acetic acid present at the bottom of the line. It is not possible to provide a constant concentration of undissociated acetic acid in the condensed water, since this depends on the pH of the droplets, which fluctuates quite a lot during the condensation process. A gradient of concentration also exists between the outer envelope of the droplets (liquid/vapor interface) and the steel surface. For clarity reasons, the concentration of acetic acid will be referred to below as the concentration of acetic acid in the liquid phase at the bottom of the line (tank water).

### Materials Characterization

All of the weight-loss coupons are made of API X-65 carbon steel prepared from the same piece of field pipe line. The chemical analysis of this X65 steel and its microstructure have been reported previously by Singer, et al.,<sup>28</sup> but are repeated in Table 4, Table 5, and Figure 2.

### Corrosion Rate Measurement

The weight-loss coupons were not inserted into the corrosion environment until the system reached steady state. The corrosion rates are measured with

weight-loss coupons made of API X65 carbon steel. Samples consisting of cylindrical coupons (0.76 cm internal diameter, 3.17 cm external diameter, and 0.5 cm thickness) with an exposed area of 7.44 cm<sup>2</sup> are polished using isopropanol as coolant on silicon carbide papers up to 600 grit. After this preparation, they are covered with a protective coating on the outer edges and bottom (Figure 3). Following 4 h to 6 h of curing at ambient conditions, the samples are held at 200°C in an oven for 4 h. The uncovered steel surface is then re-polished with 600 grit silicon carbide paper wetted with isopropanol, cleaned, dried, and weighed. The coupons then are flush-mounted on the internal pipe wall of the loop by using a specially designed probe holder (Figure 3). Therefore, only one face of the coupon is in direct contact with the corrosive environment. The exposure time is between 2 days and 21 days in all experiments. Upon removal from the loop, the coupon surface is flushed with isopropanol to dehydrate it. Then, photographs of the surface are taken. The weight of the coupon after each test is registered, and the ASTM G1<sup>29</sup> standard procedure is followed to remove the corrosion products and determine the corrosion rate by weight loss. Some coupons

**TABLE 4**  
*Chemical Analysis of the Carbon Steels  
Used in the Experiments*

Element	X65 Composition (%)	API 5L X65 Standard (%)
C	0.13	<0.26
Mn	1.16	<1.40
P	0.009	<0.03
S	0.009	<0.03

are preserved for corrosion product evaluation by scanning electron microscopy (SEM) and energy-dispersion analysis (EDS).

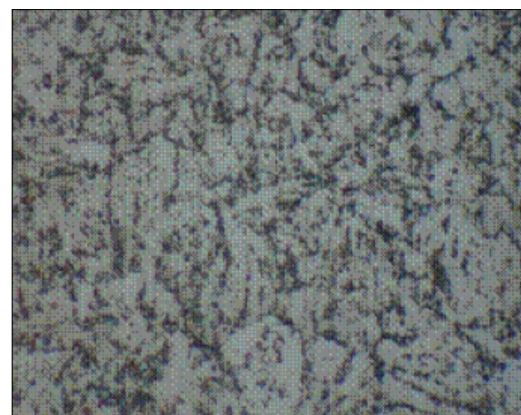
It is important to mention that, using this method, the corrosion rate at any point in time represents an integration of the corrosion rate profile prior to that point. Considering that the corrosion rate after 2 days of exposure is often 3 to 5 times higher than it is after 21 days, the “weight loss” corrosion values overestimate the actual “real time” rates, especially toward the end of the test. Differential corrosion rates could be calculated to address this issue, but the scatter in the results leads to large fluctua-

**TABLE 5**  
*Hardness (HRB) Results*

	X65 Longitudinal Cut	X65 Transversal Cut
1	81.3	60.3
2	94.4	68.7
3	98.7	63.3
4	87.9	78.0
5	95.4	59.1
6	89.3	51.1
7	88.7	66.5
8	92.9	75.0
9	93.3	58.5
10	85.1	67.7
Average	90.7	64.8
Approx. tensile strength	90,000 psi for 90.7HRB	56,000 psi for 65.7HRB
Tensile requirements	77,000 psi (min)	77,000 psi (min)
Yield strength	65,000 psi (min)	65,000 psi (min)



(a) 1,000X



(b) 1,000X

**FIGURE 2.** Microstructure of the X65 carbon steel: (a) longitudinal cut and (b) transversal cut.

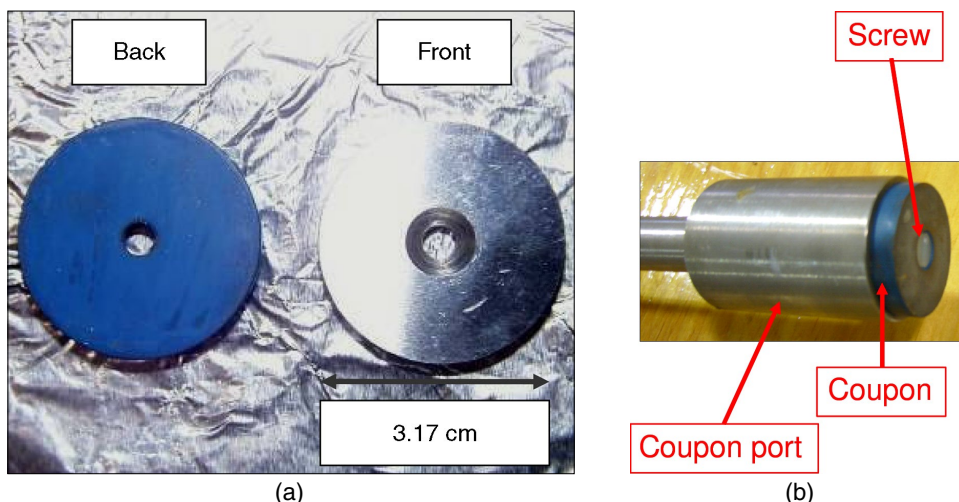


**FIGURE 3.** Weight-loss coupon design: (a) weight loss coupons with PTFE coating on the back and the side and (b) coupon holder configuration.

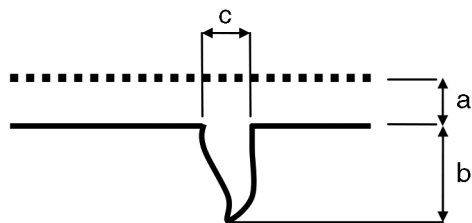


**FIGURE 4.** Schematic representation of pitting corrosion: (a) general corrosion depth, (b) pit depth after film removal, and (c) diameter of pit after film removal.

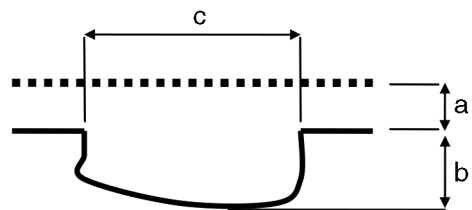


**FIGURE 5.** Schematic representation of mesa attack: (a) general corrosion depth, (b) pit depth after film removal, and (c) diameter of pit after film removal.

tions, which do not, in the author's opinion, help in the understanding. However, this calculation artifact should be kept in mind in the results analysis.

### Localized Corrosion Characterization

Information on the occurrence and extent of localized corrosion is collected for each test performed using a 3D surface profilometer. It is therefore important to define clearly the parameters measured.

**Pitting Corrosion** — Generally, pits are deep and narrow, and either hemispherical or cup-shaped. When pitting corrosion happens, a part of the material surface undergoes rapid attack while most of the adjacent surface remains unaffected. As described in

Figure 4, the criteria used to define pitting corrosion are displayed below:

- the pit depth is five times deeper than the general corrosion depth ( $b \geq 5a$ ),
- the diameter of pit after film removal is smaller than the pit depth ( $c \leq b$ ).

**Mesa Attack** — Mesa attack is characterized by a wide and often flat-bottomed local attack without protective corrosion film, surrounded by areas with intact corrosion films. Generally, mesa attack starts as several small pits growing beneath the corrosion film. These pits continue to grow beneath the corrosion layer, both laterally and in-depth, and can coalesce into wide, flat-bottomed features. The corrosion product layer on top of the mesa attack often collapses either because of internal stresses or flow effects. A galvanic effect between the film-free corroding metal in the bottom of the mesa attack and the film-covered steel outside the mesa attack can increase the corrosion rate in the mesa attack area. As described in Figure 5, the criteria used for mesa attack are:

- the mesa attack depth is five times bigger than general corrosion depth ( $b \geq 5a$ ),
- the diameter of mesa is bigger than pit depth ( $c \geq b$ ).

**Percentage of Coupon Surface Affected by Localized Corrosion** — Since weight-loss steel coupons are used in this study, it was found that the percentage of the coupon surface affected by localized corrosion (pitting and mesa attack together) constitutes an indication of the likelihood of its occurrence.

An example of the analysis performed on each steel sample is shown in Figure 6. The method of differentiation is shown with the data used to determine the percentage of the steel surface area affected by localized corrosion. Rates of localized corrosion are calculated by dividing the feature depth (average or maximum) by the exposure time, and are given in mm/y.

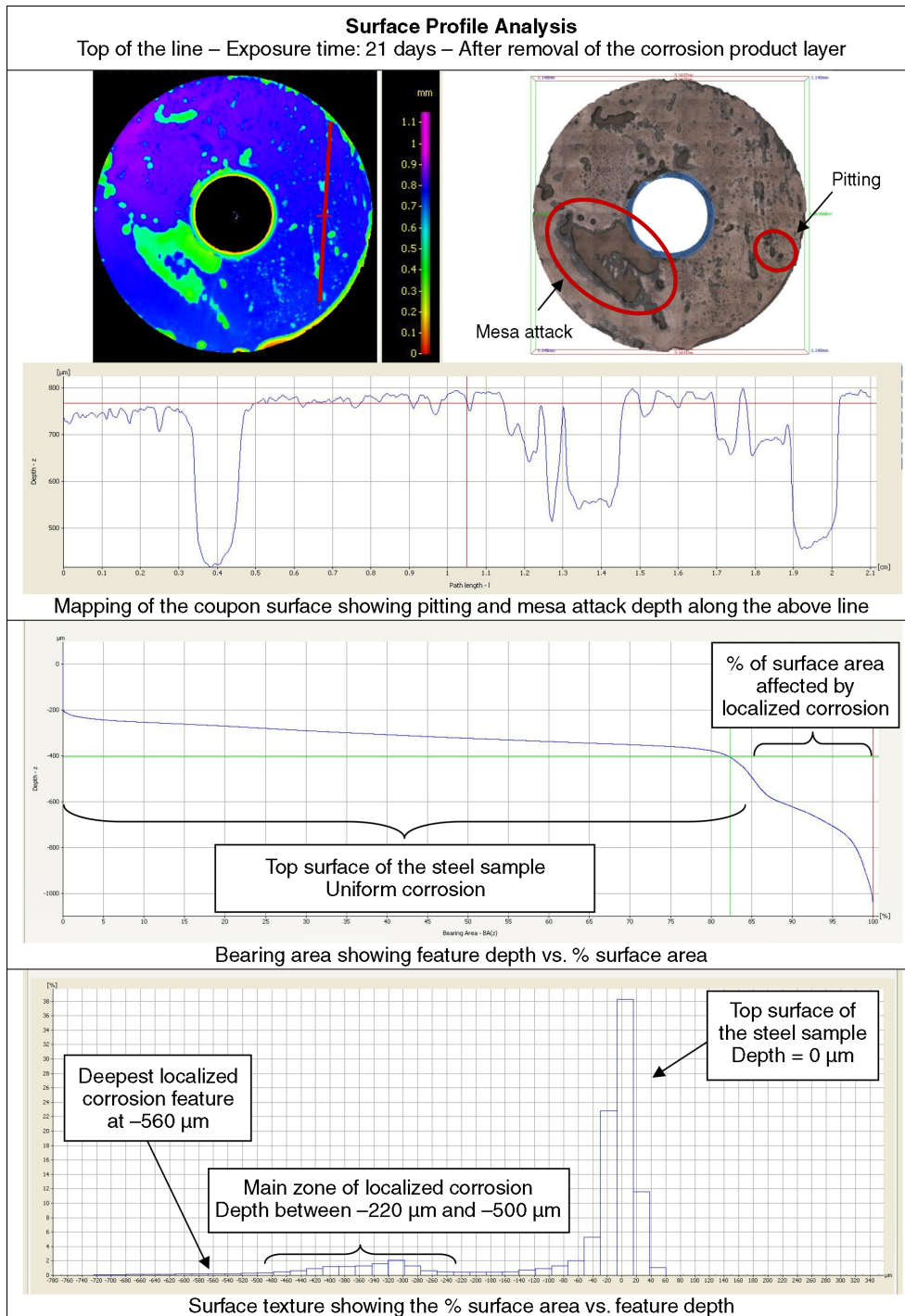


**FIGURE 6.** Analysis of pitting and mesa attack.  $[HAc]_{free} = 1,000 \text{ mg/L}$  and condensation rate =  $1 \text{ mL/m}^2/\text{s}$ . ( $p_T$ : 3 bars,  $V_g = 5 \text{ m/s}$ ,  $p_{CO_2} = 2 \text{ bars}$ ,  $T_g$ :  $70^\circ\text{C}$ ).

### Experimental Design Flaws and Disclaimer

No laboratory setup can represent perfectly the conditions in the field. While pure corrosion issues have been simulated successfully in small-scale setups, the flow conditions relative to a 30 in (0.76 m) ID pipeline are not easily reproducible. TLC is actually as much a corrosion issue as it is a flow regime and heat-transfer issue. TLC occurs only in stratified flow,

but the way that the condensation process occurs at the top of the line (forming a thin flowing liquid film, or a bigger stagnant droplet) is of prime importance. As was done in this study, using flat weight-loss coupons flush-mounted to a cylindrical 4 in ID pipe creates conditions leading to preferential condensation and areas where the condensed liquid is trapped artificially (especially at high gas velocity). On the

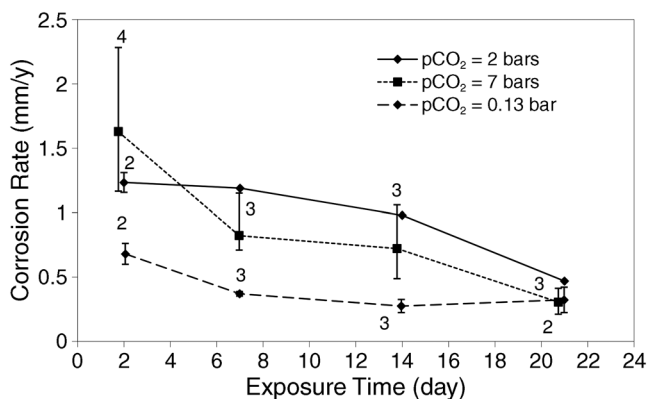


FIGURE 7. Average corrosion—Effect of  $p\text{CO}_2$ .  $T_g = 70^\circ\text{C}$ ,  $[\text{HAc}]_{\text{free}} = 0 \text{ mg/L}$ ,  $V_g = 5 \text{ m/s}$ , condensation rate =  $0.25 \text{ mL/m}^2/\text{s}$ .

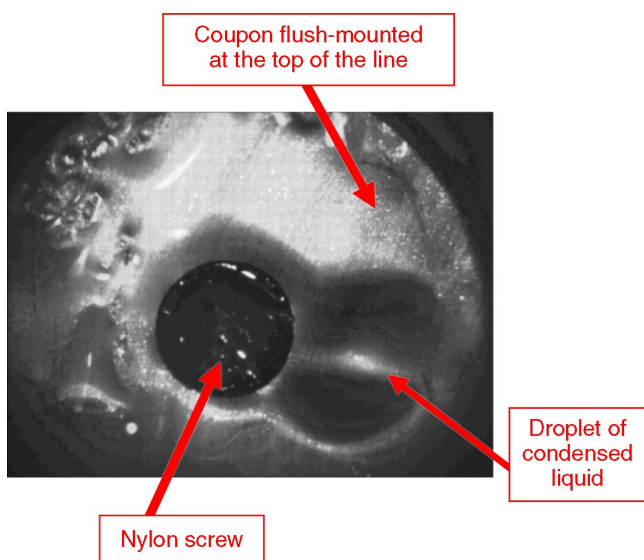


FIGURE 8. View of the weight-loss coupon at the beginning of test taken via a port installed at the bottom of the line.

other hand, using long carbon steel spool pieces is a better representation of the field conditions but is also inconvenient and more costly. In addition, the condensation process happening at the top of a 30 in ID pipeline cannot be reproduced perfectly by a 4 in ID spool piece because the wall curvature is quite different, leading to unrealistic wetting properties (filmwise instead of dropwise condensation, shorter droplet residence time). This would lead to an unrepresentative corrosion scenario. In conclusion, the approach presented in this paper, while being better and more realistic than most previous attempts, has the inconvenience of creating “edge” effects in certain conditions. Notwithstanding, the authors believe that the key effects of each influential parameter were determined successfully, but advise that the numerical values of corrosion rate should be used with caution, because they are probably conservative estimates.

## RESULTS

This chapter presents the corrosion rate results obtained for each of the tests performed. Two types of information are discussed: the evolution of the average corrosion rate with time and the occurrence of localized corrosion. The average corrosion rate is calculated using the weight loss of a coupon and the time of exposure. This provides a time-averaged corrosion rate over the entire period of exposure. The localized corrosion data present corrosion rates from pitting or mesa attack and indicate the percentage of surface area of the coupon affected. The corresponding values are obtained by performing a surface analysis on each coupon with a 3D surface profilometer.

The corrosion rate results are displayed in a series of graphs from Figures 7 through 20. The error bars represent the experimental range (minimum and the maximum values) obtained, and the number of coupons (i.e., the number of repeated measurements) is displayed, when applicable, on each graph.

In  $\text{CO}_2$  TLC, the average corrosion rate usually starts at a high value (several millimeters per year) but in almost every case decreases with time, even over a period of a few weeks. This is a result of the accumulation of  $\text{Fe}^{2+}$  and the consequent rise in pH in the droplet, which can lead to the formation of  $\text{FeCO}_3$  on the metal surface, once  $\text{FeCO}_3$  saturation is reached. However, although the average corrosion rate usually is decreased significantly, the relative protectiveness of this layer with regard to localized corrosion will be affected by the experimental conditions, especially the concentration of acetic acid or condensation rate.

### Influence of the $\text{CO}_2$ Partial Pressure

In general, the higher the partial pressure of  $\text{CO}_2$ , the higher the average corrosion will be, as shown in Figure 7. A protective  $\text{FeCO}_3$  film forms on the surface of the coupon and leads to a decline of the corrosion attack after 18 days of testing at 2 bars partial pressure of  $\text{CO}_2$  and above. At lower partial pressure of  $\text{CO}_2$  (0.13 bar), the conditions of  $\text{FeCO}_3$  supersaturation (saturation in  $\text{FeCO}_3$  above unity) seem to be more difficult to reach, and the protective film does not form correctly, leading to a low but constant corrosion rate over time (around 0.4 mm/y). At higher partial pressure of  $\text{CO}_2$ , the corrosion attack is initially more aggressive, but the average corrosion rate decreases with time to reach 0.3 mm/y after 21 days of testing. Since the conditions of  $\text{FeCO}_3$  supersaturation are met easily (high  $\text{Fe}^{2+}$  and  $\text{CO}_3^{2-}$  concentration), a dense protective film forms on the metal surface. Pitting corrosion was observed at partial pressures of 2 bars and 7 bars, and stronger at 7 bars partial pressure of  $\text{CO}_2$  (Table 6). Weaker pitting was observed at 0.13 bars partial pressure of  $\text{CO}_2$  after 21 days of testing. In the case of  $\text{CO}_2$  TLC, the occurrence of

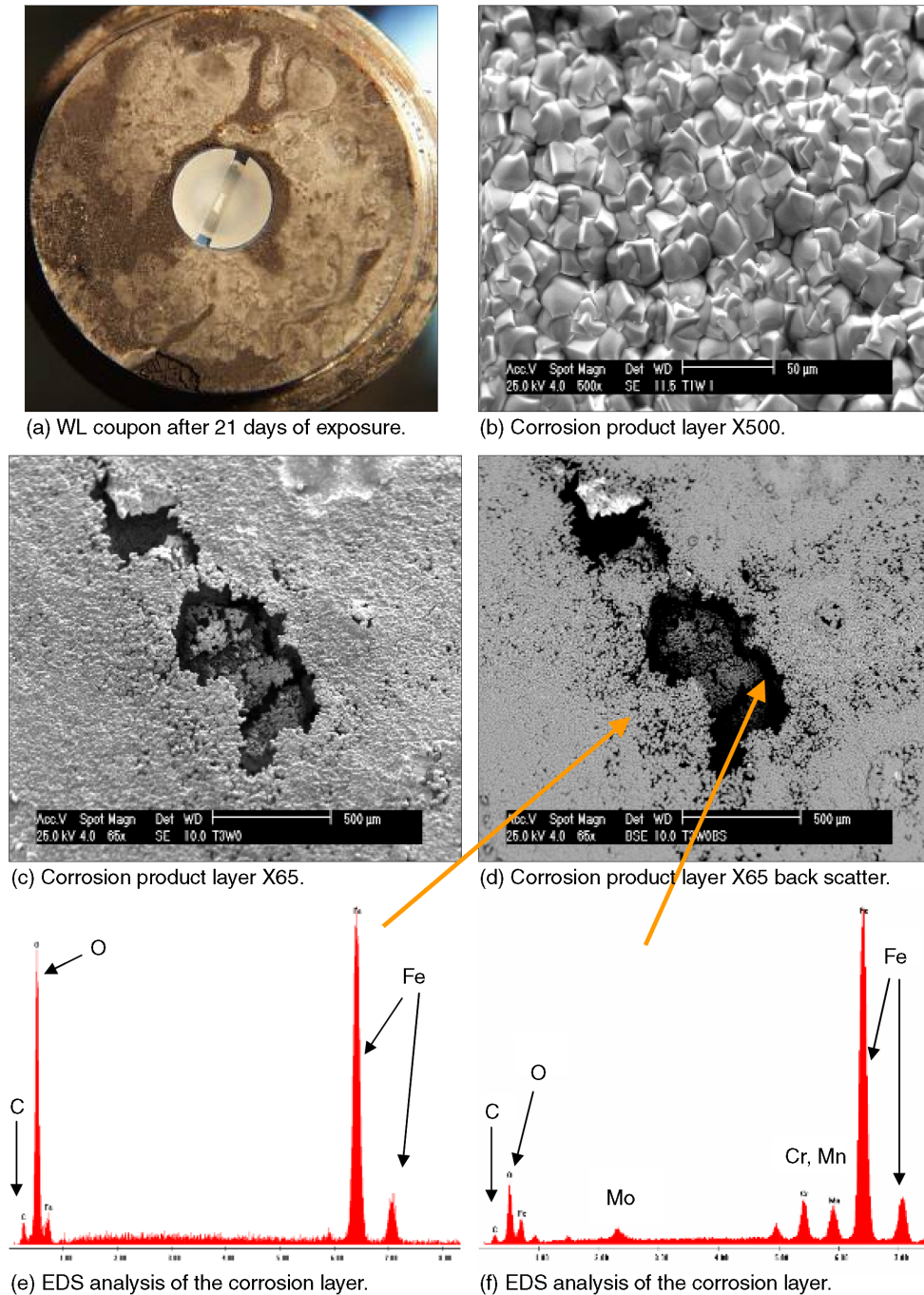


**FIGURE 9.** Surface analysis with corrosion product/ $p\text{CO}_2 = 2$  bars. (PT: 3 bars,  $V_g = 5$  m/s,  $[\text{HAc}]_{\text{free}}: 0$  mg/L,  $T_g: 70^\circ\text{C}$ , condensation rate =  $0.25$  mL/m<sup>2</sup>/s)

localized corrosion is strongly linked with the presence of a protective  $\text{FeCO}_3$  layer, which undergoes some breakdown as a result of higher local corrosivity. The change in corrosivity in the condensed liquid is because of the condensation process itself, which sees droplets of liquid nucleate grow and eventually fall because of gravity forces. During this process, the chemistry in the droplet undergoes a significant increase in pH and in  $\text{Fe}^{2+}$  concentration, which favors local scale formation. Once the droplet reaches its maxi-

mum size and falls, a new droplet will form with lower pH and more aggressive corrosiveness. The cycle is believed to challenge the protectiveness of the  $\text{FeCO}_3$  layer and lead to localized corrosion (Figure 9).

#### *Influence of Gas Velocity*

The most visible influence of gas velocity appears on the condensation regime, which, in return, will affect the way the corrosion process occurs. At low velocity ( $<5$  m/s), the vapor condenses by forming

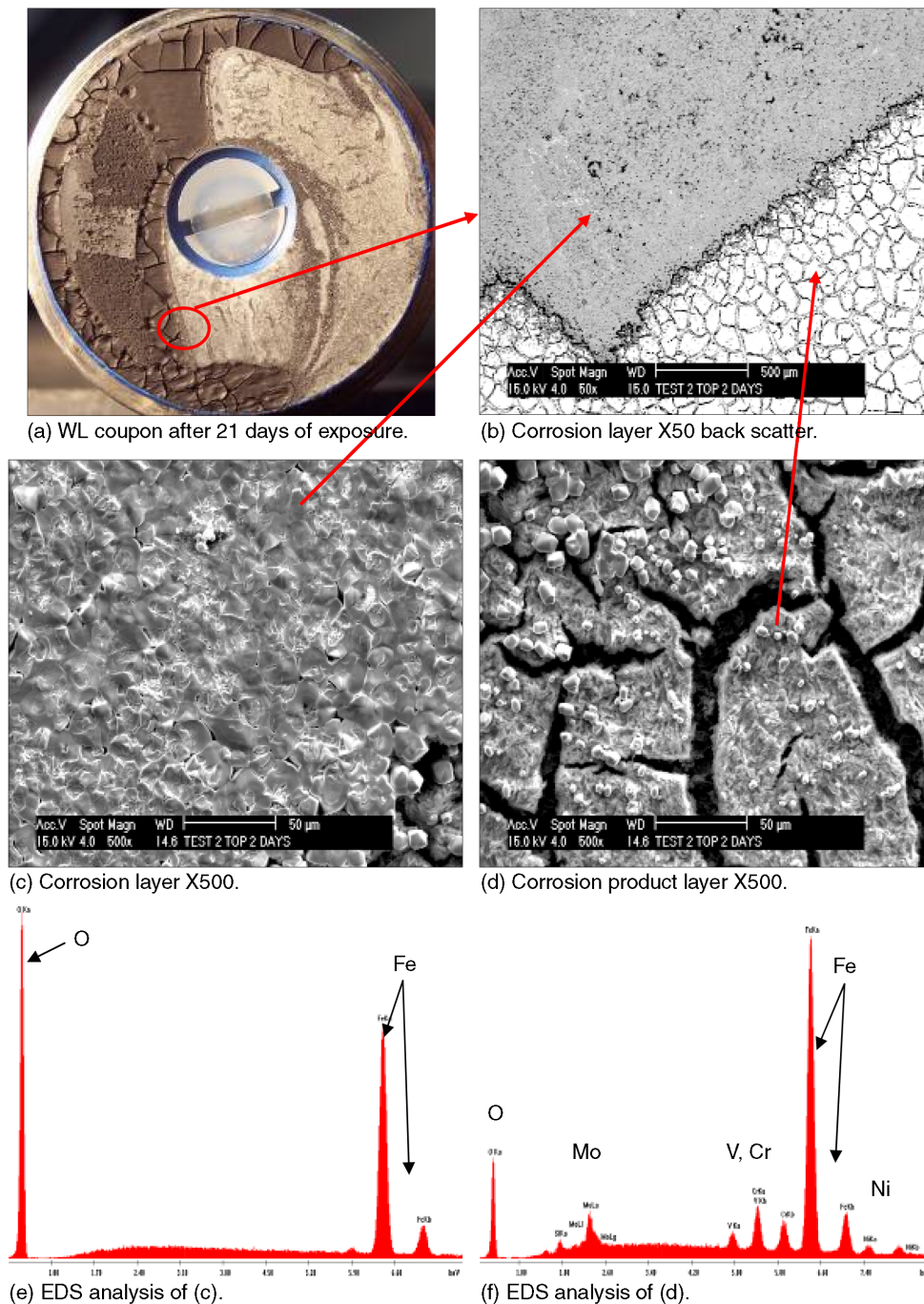


**FIGURE 10.** Surface analysis with corrosion product/ $V_g = 10$  m/s. (PT: 3 bars,  $pCO_2$ : 2 bars, free HAc: 0 mg/L,  $T_g$ : 70°C, condensation rate = 0.25 mL/m<sup>2</sup>/s).

stagnant droplets at the top of the pipe (Figure 8). In these stagnant droplets, it is foreseen that the  $FeCO_3$  supersaturation can be reached rather easily, especially at a low water condensation rate, enabling the formation of a dense protective layer. As the gas velocity increases, the condensation regime switches gradually from stagnant to sliding droplet. In the sliding droplet mode, the droplets of condensed liquid flow along the top of the pipe and can slide to the sides of the pipe, eventually reaching the bottom. In a real

field environment, there should not be any fundamental differences between sliding and stagnant droplets, as they both would be saturated rapidly with corrosion products. However, in this specific experimental setup, most of the droplets sliding along the pipe come from upstream of the carbon steel sample area and do not contain any corrosion product (i.e., they are comprised of fresh acidic water), since the rest of the pipe is made of stainless steel and does not corrode. Consequently, as the sliding droplets flow on

the sample surface, they are not generally in contact with the steel long enough to create a  $\text{FeCO}_3$  film (as opposed to the stagnant droplet condensation regime). Instead, a thick but non-protective  $\text{Fe}_3\text{C}$  forms on the liquid pathways that the sliding droplets create. It leads to the formation of two different types of layers at the top of the line: protective  $\text{FeCO}_3$  on most of the coupon area and non-protective  $\text{Fe}_3\text{C}$  on the preferential liquid pathways. Figure 10 clearly shows these preferential liquid pathways at a gas velocity of 10 m/s. Again, this is an artifact of the experimental setup but also could represent real field situations, such as transition zones between corrosion-resistant alloy/carbon steel pipe sections.

The weight-loss method does not differentiate between the types of film and gives an average corrosion rate over the entire surface of the coupons. It is possible to correct the space average corrosion rate by evaluating the percentage of surface coverage of both types of film on the coupon surface. However, this process can lead to a high margin of error and does not bring any valuable additional information. Under the  $\text{Fe}_3\text{C}$  layer, the average corrosion rate can be as high as 10 mm/y (similar to what would happen at the bottom of the line). Under the parts of the coupons covered by a  $\text{FeCO}_3$  layer, the situation resembles a typical TLC scenario with a much lower average corrosion rate. Some localized corrosion was observed in every test on the parts covered by  $\text{FeCO}_3$ . The corrosion under  $\text{Fe}_3\text{C}$  film is usually uniform. There was no clear influence of the gas velocity on the extent of the localized corrosion. The space average corrosion rate results do not appear in this paper since they do not help in clarifying this particular phenomenon. There was no visible effect of the gas velocity on the TLC (uniform and localized corrosion) except for the change in condensation regime discussed earlier.

Observation of the transition between stagnant and sliding condensation regimes was made possible by the presence of a high-pressure, high-temperature video camera installed at a bottom port of the test section, enabling the in situ visualization of the corrosion process occurring on the sample surface. In the conditions tested (total pressure of 3 bars, gas temperature of 70°C, gas phase made of  $\text{CO}_2$  and water vapor), the transition between the two condensation regimes was observed at a gas velocity around 10 m/s. Since then, a more comprehensive effort to understand and predict the transition zone between stagnant and sliding droplet regimes has been made. A model developed by Zhang, et al.,<sup>22</sup> was presented in 2006 and constitutes a good predictive tool for this kind of scenario.

In summary, once the condensation regime switches from stagnant to sliding droplet, parts of the coupon at the top of the line start to be heavily corroded at a rate similar to that at the bottom of the line. However, the flow regime is not yet annular

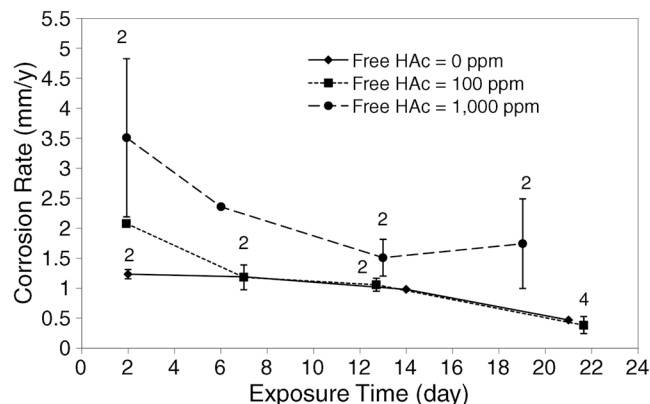
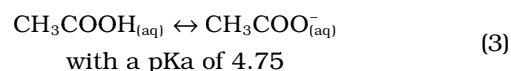


**FIGURE 11.** General corrosion—Effect of the free HAC concentration.  $p\text{CO}_2 = 3$  bars,  $T_g = 70^\circ\text{C}$ , condensation rate = 0.25 mL/m<sup>2</sup>/s,  $V_g = 5$  m/s.

(which happens in experimental conditions around 20 m/s) because the droplets flowing at the top are still made exclusively of pure condensed water saturated with  $\text{CO}_2$ . Defining this transition zone is therefore quite important. Additional issues related to droplet transport from the bottom to the top of the line may be expected at high gas velocity. However, no inquiry was made into this phenomenon during the study.

### Influence of the Concentration of Undissociated Acetic Acid

The presence of 100 mg/L of free acetic acid in the liquid phase of the tank does not seem to have a strong impact on the average corrosion rate (Figure 11). The contribution to the overall cathodic reaction of such a relatively small amount is also minimal. However, as the free acetic acid concentration is increased to 1,000 mg/L, the average corrosion rate doubles at each point in time. The corrosion rate was still at 2 mm/y after 3 weeks of testing. Moreover, the presence of acetic acid strongly promotes the occurrence of pitting corrosion, proportionally to the amount of acid in the solution (Table 6). With 1,000 mg/L of free acetic acid, the pitting rate was 7.5 mm/y after 3 weeks of testing. Once again, the presence of a corrosion product layer together with a local change in chemistry and pH (because of the continuous renewal of condensed droplets) are believed to be responsible for the occurrence of localized corrosion. Acetic acid, being a volatile weak acid, increases the corrosivity of the condensed water and challenges the integrity of the  $\text{FeCO}_3$  layer (Figure 12). It dissociates according to the following reaction:



Acetic acid consequently acts as a reservoir of protons and contributes, as carbonic acid, to the buff-

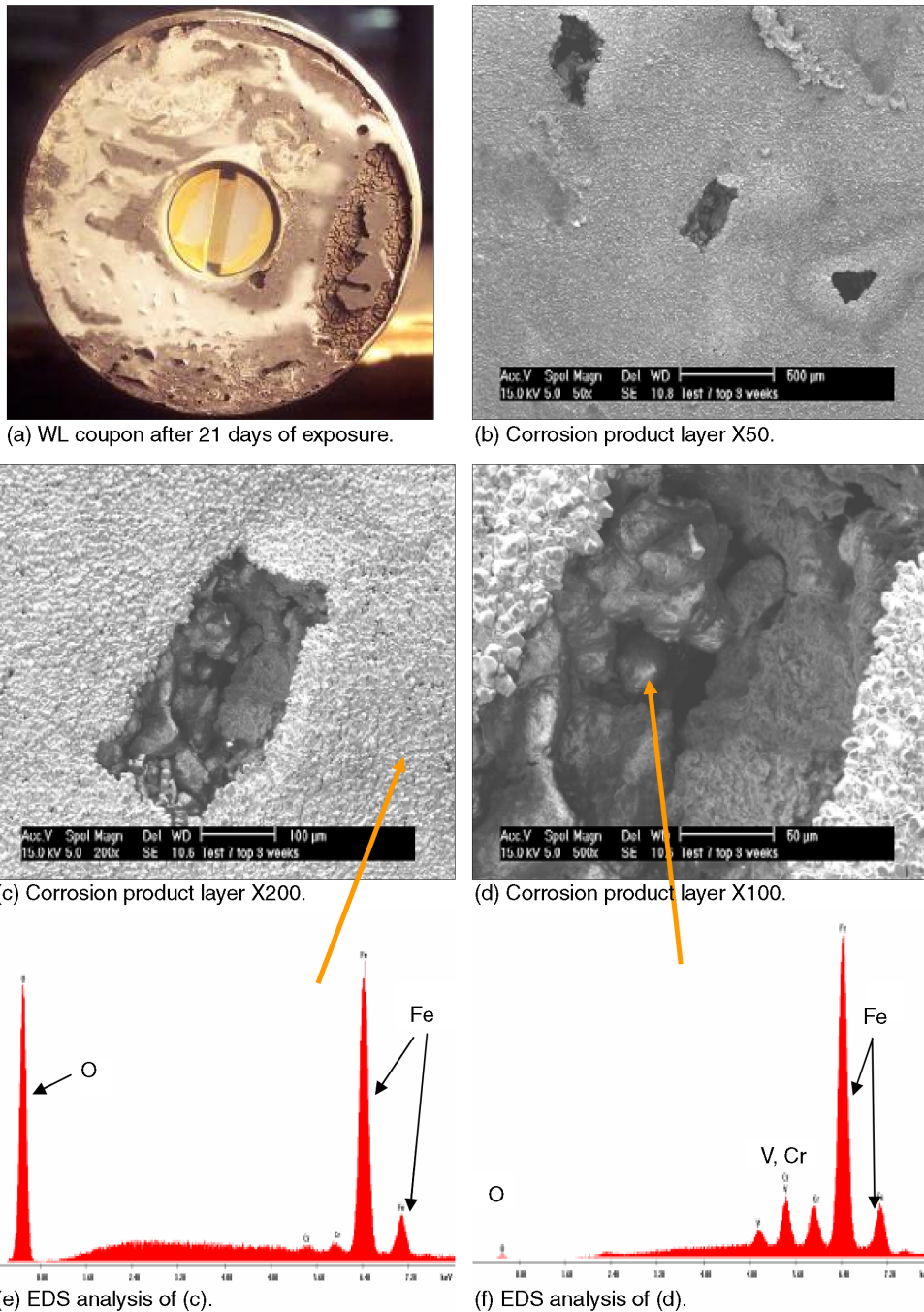


**FIGURE 12.** Surface analysis with corrosion product/free HAC = 1000 mg/L. (PT: 3 bars,  $V_g = 5$  m/s,  $p\text{CO}_2 = 2$  bars,  $T_g: 70^\circ\text{C}$ , condensation rate =  $0.25$  mL/m<sup>2</sup>/s).

ering of the solution pH. This, in turn, affects the  $\text{FeCO}_3$  saturation level, especially close to the metal surface where the precipitation reaction occurs.

#### *Influence of the Condensation Rate*

The average corrosion rate is expected to be lowest at the lowest condensation rate (Figure 13). The reason is that the rate of renewal of condensed droplets is faster at higher condensation rates. The saturation of  $\text{FeCO}_3$  is easier to achieve when droplets of

liquid remain attached to the metal surface for a longer time. This behavior has been observed clearly in the field, as numerous authors have reported.<sup>2,3,5</sup> Nevertheless, the effect of the water condensation rate was not always clear in the conditions tested. The final average corrosion rate is about twice as high at  $1$  mL/m<sup>2</sup>/s compared to  $0.03$  mL/m<sup>2</sup>/s, but the overall trend is rather similar in all cases (especially at  $1$  mL/m<sup>2</sup>/s and  $0.25$  mL/m<sup>2</sup>/s). A stronger contrast was expected, since a higher condensation rate is

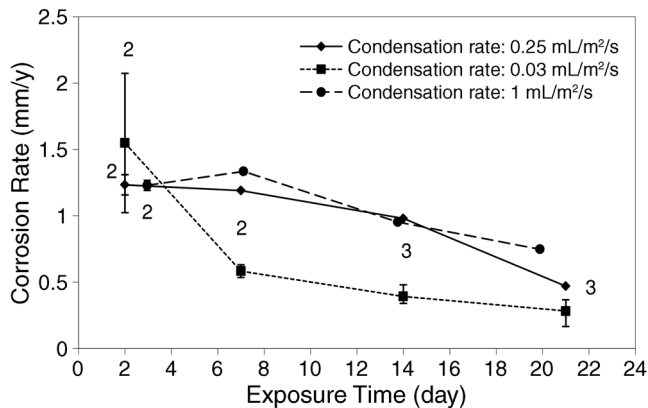


**FIGURE 13.** General corrosion—Effect of the condensation rate.  $p\text{CO}_2 = 3 \text{ bars}$ ,  $T_g = 70^\circ\text{C}$ ,  $[\text{HAc}]_{\text{free}} = 0 \text{ mg/L}$ ,  $V_g = 5 \text{ m/s}$ .

usually synonymous with a higher general corrosion rate. In all cases, the condensation regime seems to be stagnant droplet condensation. The lack of stronger influence on the average corrosion rate is thought to be because of the specific design of the sample holder. As mentioned previously, using flat weight-loss coupons flush-mounted to a cylindrical 4 in ID pipe leads to areas on the samples where condensed water is artificially “trapped,” which could have masked the effect of the condensation rate. However, it is clear that the influence of the condensation is much stronger on the localized attack (Table 6). Both pitting rate and surface coverage by localized attack increase dramatically with the condensation rate. Figure 14 shows one of the weight-loss coupons exposed for 21 days to the baseline environment and a condensation rate of  $1 \text{ mL/m}^2/\text{s}$ . The corrosion product layer has been removed and the steel surface presents numerous localized corrosion features. Mesa attack seems to be predominant in this case with wide pits easily identifiable.

### Influence of the Gas Temperature

Since the corrosion reactions respond to temperature according to Arrhenius-type laws, the average corrosion rate decreases as the gas temperature decreases (Figure 15). This is usually true in full pipe flow, where there is no protective film forming at the surface of the steel. It is, however, different at the top of the line, as the presence of a protective layer plays a role as well. In the first days of testing, the corrosion rate was higher at a higher temperature ( $70^\circ\text{C}$  compared with  $40^\circ\text{C}$ ). However, as time goes by, the corrosion rate at  $70^\circ\text{C}$  decreases strongly, while the corrosion rate at  $40^\circ\text{C}$  does not. After 15 days, the corrosion rate at  $70^\circ\text{C}$  test reached the same value as  $40^\circ\text{C}$ ; after 20 days, it stopped. In contrast, at  $40^\circ\text{C}$ , the corrosion rate started at a low value ( $0.5 \text{ mm/y}$ ) but remained almost constant throughout the test. This is explained by the properties of the film forming at the surface of the steel: a dense and protec-

tive  $\text{FeCO}_3$  layer at  $70^\circ\text{C}$  and a more porous and less-protective  $\text{FeCO}_3$  layer at  $40^\circ\text{C}$ . The same reasoning applies for the test at  $85^\circ\text{C}$ , where it started at the highest value (above  $1.5 \text{ mm/y}$ ) and strongly decreased with time to reach  $0.5 \text{ mm/y}$  after 17 days. The corrosion product film is expected to be denser and more protective at a higher temperature since the kinetics of  $\text{FeCO}_3$  precipitation are faster. Moreover, at the top of the line, there was no sign of localized corrosion at  $40^\circ\text{C}$  or  $85^\circ\text{C}$  while there was strong evidence of pitting at  $70^\circ\text{C}$  (Table 6). It is clear that the properties of the corrosion product film (rate of formation, density, integrity) are strongly linked to the occurrence of localized corrosion.

### Combined Effect of the Condensation Rate and the Acetic Acid Concentration

For clarity purposes, the results are presented in four sets of graphs, each isolating one parameter each time:

- Set 1: fixed undissociated acetic acid concentration =  $100 \text{ mg/L}$  and varying condensation rate =  $0.03$ ,  $0.25$ , and  $1 \text{ mL/m}^2/\text{s}$
- Set 2: fixed undissociated acetic acid concentration =  $1,000 \text{ mg/L}$  and varying condensation rate =  $0.03$ ,  $0.25$ , and  $1 \text{ mL/m}^2/\text{s}$
- Set 3: fixed condensation rate =  $0.05 \text{ mL/m}^2/\text{s}$  and varying undissociated acetic acid concentration =  $0$ ,  $100$ ,  $1,000 \text{ mg/L}$
- Set 4: fixed condensation rate =  $1 \text{ mL/m}^2/\text{s}$  and varying undissociated acetic acid concentration =  $0$ ,  $100$ ,  $1,000 \text{ mg/L}$

The graphs related to each set are presented in Figures 16 through 19. The clearest observation is that the higher the concentration of free acetic acid and the condensation rate are, the higher the risk for localized corrosion. Even if the condensation rate is low ( $0.05 \text{ mL/m}^2/\text{s}$ ),  $1,000 \text{ mg/L}$  of free HAc will lead to a high average corrosion rate and severe localized attack (Figure 20). The opposite is also true for the condensation rate but to a slightly lesser extent. The notion of fixed critical threshold condensation rate below which no TLC is expected (or where the TLC rate is acceptable) is not validated by these results. The water condensation rate is clearly a factor influencing the average corrosion and localized corrosion rate but should not be extracted alone and used as a design tool. This does not mean that minimizing the water condensation is not an effective method to mitigate TLC in field environments (especially  $\text{CO}_2$ -dominated environments); suitable pipe burial or thermal insulation clearly do offer significant protection against corrosion.<sup>2-3,5,11</sup> However, it should be understood that the extent of TLC is rather the result of complex interactions between all the parameters and that there is no guarantee that one single threshold value of water condensation rate will be adapted to different field conditions.

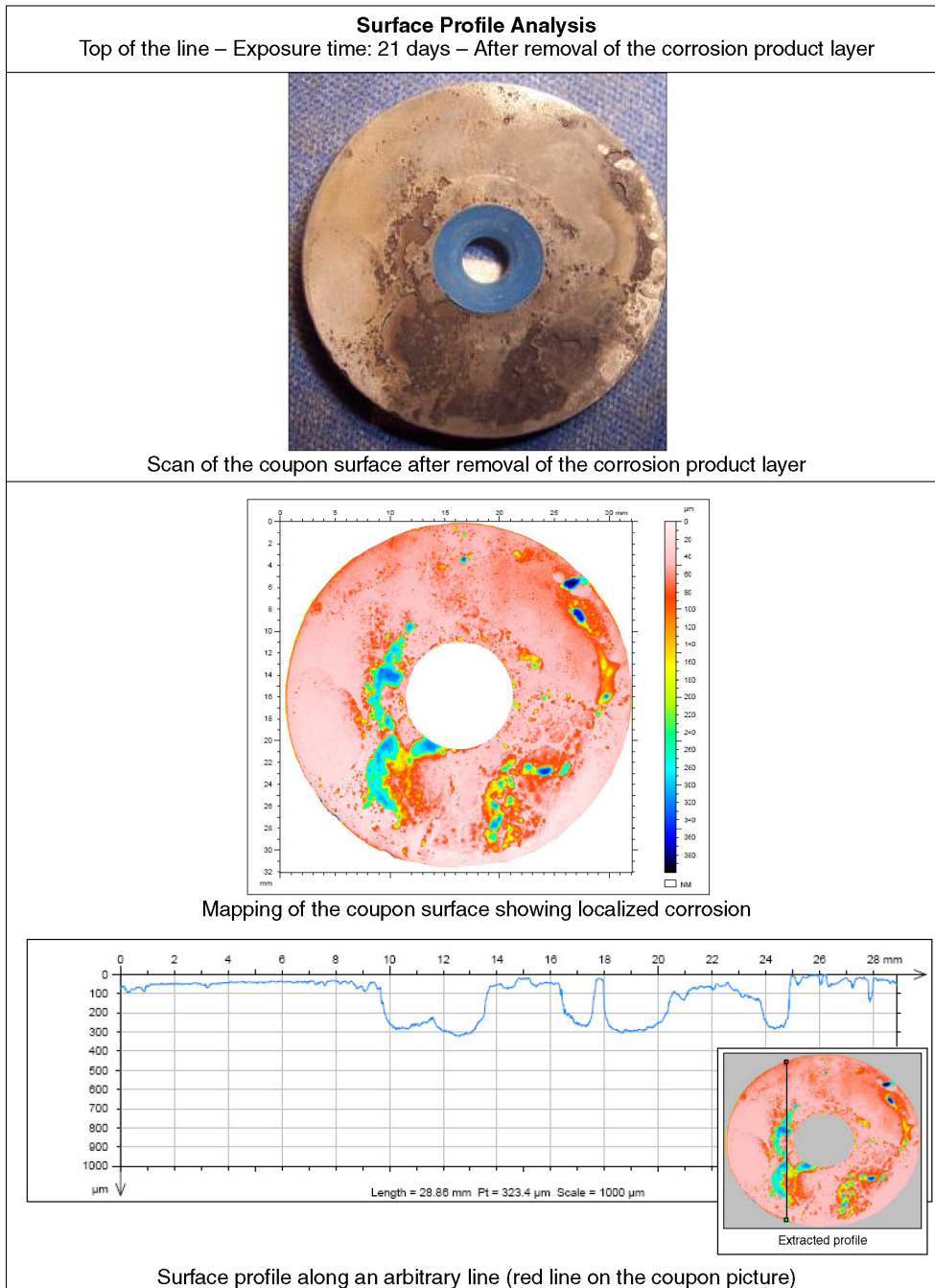


**FIGURE 14.** Surface analysis without corrosion product. Condensation rate =  $1 \text{ mL/m}^2/\text{s}$ . ( $P_T$ : 3 bars,  $V_g$  = 5 m/s,  $p\text{CO}_2$  = 2 bars,  $T_g$ :  $70^\circ\text{C}$ ,  $[\text{HAc}]_{\text{free}} = 0 \text{ mg/L}$ ).

## CONCLUSIONS

The present experimental study, performed in large-scale flow loops, highlights some important characteristics of sweet TLC. TLC is a phenomenon that occurs only in stratified flow, although two distinct condensation regimes are encountered: stagnant droplet condensation at low gas velocity and sliding droplet condensation at higher gas velocity. The water vapor condenses at the top of the line in the form of small

water droplets, which follow a specific cycle: growth to reach a critical size, falling to the bottom of the pipe because of gravity forces or sliding along the pipeline, and renewal governed by the rate of condensation. The initial average corrosion rates are normally quite high but often decrease with time to relatively low average values. This decrease is an indication of the precipitation on the metal surface of a corrosion product layer made of  $\text{FeCO}_3$ . This layer can provide some protection but is also intrinsically linked to the initia-

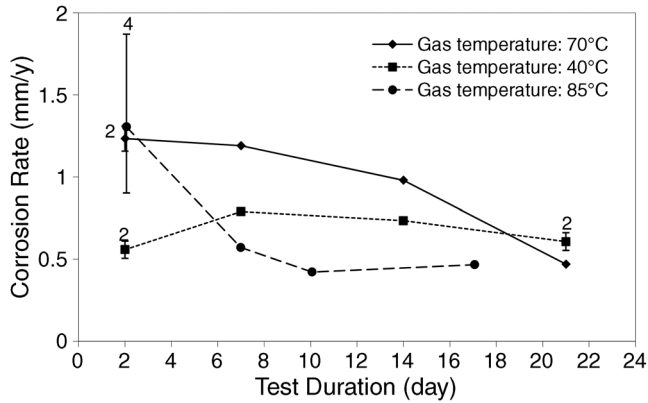


**FIGURE 15.** General corrosion—Effect of the gas temperature.  $p\text{CO}_2 = 3$  bars,  $[\text{HAc}]_{\text{free}} = 0$  mg/L,  $V_g = 5$  m/s, condensation rate =  $0.25$  mL/m<sup>2</sup>/s.

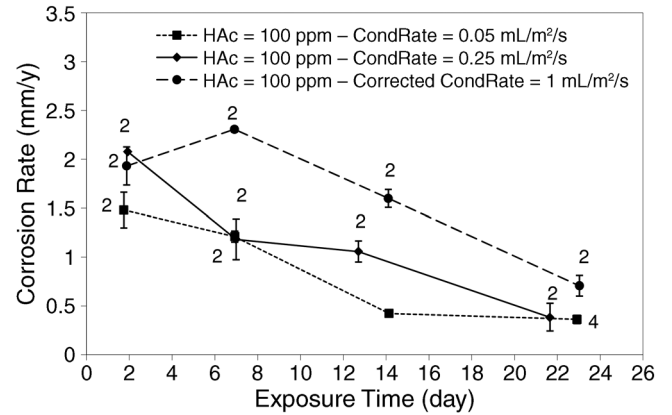


**FIGURE 16.** General corrosion—Effect of HAC/condensation rate.  $p\text{CO}_2 = 3$  bars,  $T_g = 70^\circ\text{C}$ ,  $V_g = 5$  m/s. Set 1: fixed  $[\text{HAc}]_{\text{free}} = 100$  mg/L and varying condensation rate =  $0.05$ ,  $0.25$ , and  $1$  mL/m<sup>2</sup>/s.

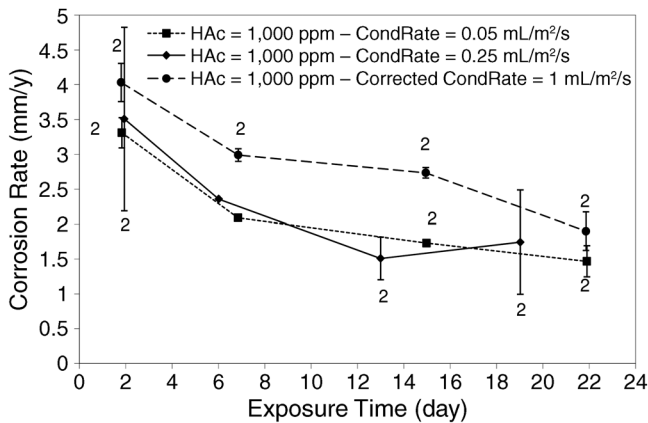


**FIGURE 17.** General corrosion—Effect of HAC/condensation rate.  $p\text{CO}_2 = 3$  bars,  $T_g = 70^\circ\text{C}$ ,  $V_g = 5$  m/s. Set 2: fixed  $[\text{HAc}]_{\text{free}} = 1,000$  mg/L and varying condensation rate =  $0.05$ ,  $0.25$ , and  $1$  mL/m<sup>2</sup>/s.

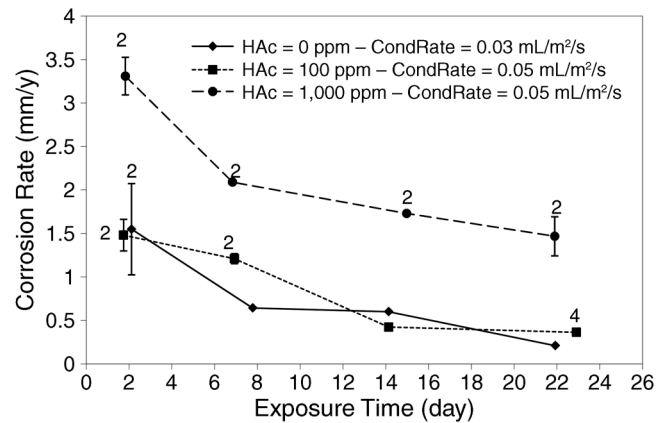


**FIGURE 18.** General corrosion—Effect of HAC/condensation rate.  $p\text{CO}_2 = 3$  bars,  $T_g = 70^\circ\text{C}$ ,  $V_g = 5$  m/s. Set 3: fixed condensation rate =  $0.05$  mL/m<sup>2</sup>/s and varying  $[\text{HAc}]_{\text{free}} = 0$ ,  $100$ ,  $1,000$  mg/L.

tion and propagation of localized corrosion. Two to three weeks of exposure time are consequently necessary to catch these tendencies, as shorter experiments may lead to unrealistically high general corrosion rates and may miss the occurrence of localized corrosion altogether. In terms of general corrosion, a more aggressive environment (high partial pressure of  $\text{CO}_2$ , higher temperature, higher acetic acid content) logically leads to higher initial corrosion rates. As the corrosion process occurs and iron ions are released in solution, the water droplets can reach saturation in  $\text{FeCO}_3$ . How quickly this saturation is reached depends upon the temperature: experiments performed at lower gas temperatures ( $<40^\circ\text{C}$ ) lead to little to no  $\text{FeCO}_3$  precipitation and a lower but uniform and relatively constant corrosion rate over time is observed. Higher gas temperatures (above  $80^\circ\text{C}$ ) seem to lead to a more rapid formation of the  $\text{FeCO}_3$  layer. The saturation level in  $\text{FeCO}_3$  also strongly depends on the water condensation, which continuously provides fresh and acidic condensed water. The cycle of droplet

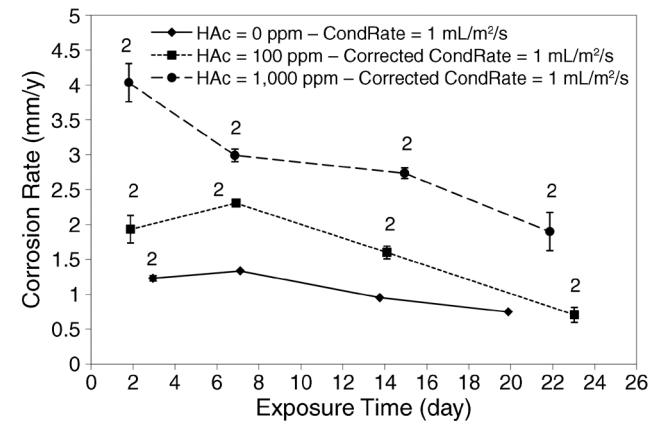


**FIGURE 19.** General corrosion—Effect of HAC/condensation rate.  $p\text{CO}_2 = 3$  bars,  $T_g = 70^\circ\text{C}$ ,  $V_g = 5$  m/s. Set 4: fixed condensation rate =  $1$  mL/m<sup>2</sup>/s and varying  $[\text{HAc}]_{\text{free}} = 0$ ,  $100$ ,  $1,000$  mg/L.

renewal greatly affects the chemistry in the condensed water (pH,  $\text{FeCO}_3$  saturation level) and challenges the protectiveness of the  $\text{FeCO}_3$ , which seems to be sub-

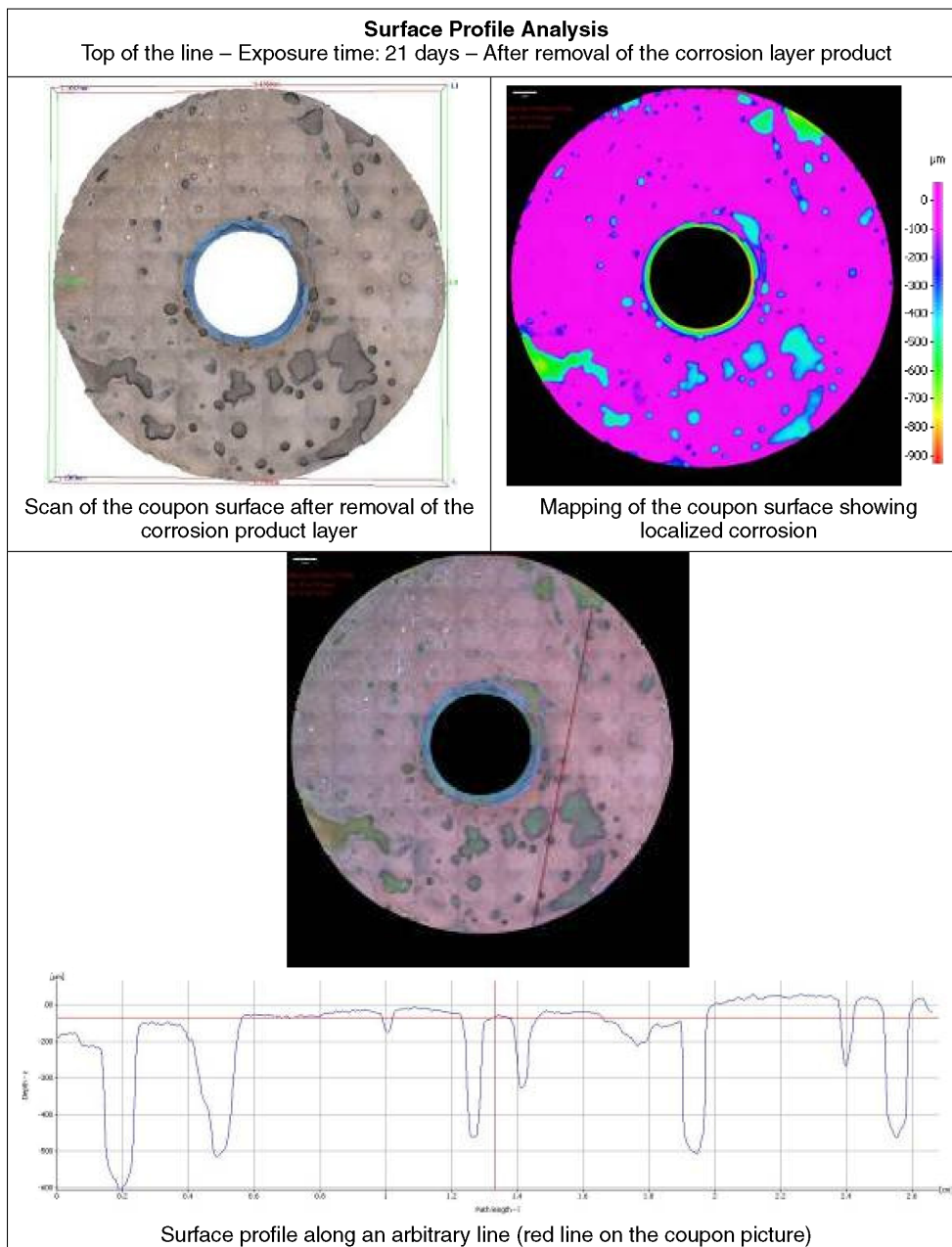


**FIGURE 20.** Baseline conditions surface analysis without corrosion product. Free HAc = 1,000 mg/L and condensation rate = 0.05 mL/m<sup>2</sup>/s. ( $P_T$ : 3 bars,  $V_g$  = 5 m/s,  $pCO_2$  = 2 bars,  $T_g$ : 70°C).

stantially weakened by high acidity (provided by CO<sub>2</sub> but especially acetic acid). Higher water condensation rates also prevent the formation of a stable corrosion product layer and strongly affect the extent of localized corrosion. Small pits are generally observed at the initial stages of the corrosion process and seem to grow together into wide, flat-bottomed mesa attacks, which can affect rather large parts of the steel sample surface area. Very high localized corrosion rates, often reaching 10 mm/y to 12 mm/y, are measured in the presence of 1,000 mg/L of acetic acid or at water condensation of 1 mL/m<sup>2</sup>/s. Under certain conditions,

localized corrosion can be limited, such as at low condensation rates (<0.05 mL/m<sup>2</sup>/s), but only with little or no acetic acid present. In all conditions tested, the presence of a large concentration of acetic acid always leads to tremendous localized corrosion rates, however low the water condensation rate might be. The extent of TLC is definitively the result of complex interactions among all of these parameters. Threshold values, often used as engineering guidelines in the industry, should be used with caution, and a solid understanding of the mechanisms involved is a prerequisite for the development of effective TLC inhibition programs.

**TABLE 6**  
Summary of General and Localized Corrosion Results (Exposure Time: 3 weeks)

Investigating	Acetic Acid		WCR		pCO <sub>2</sub>		Gas Temp.		Acetic Acid/WCR				
<b>General Experimental Conditions</b>													
Gas temperature (°C)	70	70	70	70	70	70	70	<b>40</b>	<b>85</b>	70	70	70	70
Gas velocity (m/s)	5	5	5	5	5	5	5	5	5	5	5	5	5
pCO <sub>2</sub> (bar)	2	2	2	2	2	<b>0.13</b>	<b>7</b>	2	2	2	2	2	2
pH <sub>2</sub> S (bar)	0	0	0	0	0	0	0	0	0	0	0	0	0
Free HAc in the tank (mg/L)	0	<b>100</b>	<b>1,000</b>	0	0	0	0	0	0	<b>100</b>	<b>100</b>	<b>1,000</b>	<b>1,000</b>
Condensation rate (mL/m <sup>2</sup> /s)	0.25	0.25	0.25	<b>0.03</b>	<b>1</b>	0.25	0.25	0.25	0.25	<b>0.05</b>	<b>1</b>	<b>0.05</b>	<b>1</b>
Style type	X65	X65	X65	X65	X65	X65	X65	X65	X65	X65	X65	X65	X65
<b>General Corrosion Over the Entire Sample Surface Area</b>													
Corrosion rate (mm/y)	0.5	0.4	2.5	0.2	0.8	0.4	0.3	0.6	0.5	0.4	0.7	1.5	1.9
<b>Pitting Corrosion</b>													
Average pitting rate (mm/y)	2.3	3.4	7.3	2.6	4.4	3.2	4.9	0	0	3.5	6.9	6.7	6.3
Max pitting rate (mm/y)	4.3	5	9.8	5.2	6.6	5	6.6	0	0	5.2	8.7	8.3	7.5
<b>Mesa Attack</b>													
Average mesa rate (mm/y)	5.6	3.4	9.6	2.6	6.2	3.5	6.6	0	0	0	7	6.7	6.7
Max mesa attack (mm/y)	6.3	5	12.3	3.5	7	4.7	8.2	0	0	0	8.7	10.8	9.2
<b>Percentage of Sample Surface Area Affected by Localized Corrosion (Mesa + Pitting)</b>													
% of surface area	3.7	2	17.2	1.6	14.1	4.1	4	0	0	0.5	7	11.6	14.2

## REFERENCES

1. R. Paillassa, M. Dieumegard, M. Estevoyer, "Corrosion Control in the Gathering System at Lacq Sour Gas Field," in Int. Congress of Metallic Corrosion (Houston, TX: NACE International, 1963), p. 410-417.
2. Y. Gunaltun, D. Supriyataman, A. Jumakludin, "Top of the Line Corrosion in Multiphase Gas Line, A Case History," CORROSION/1999, paper no. 36 (Houston, TX: NACE International, 1999).
3. Y. Gunaltun, D. Supriyataman, J. Achmad, *Oil Gas J.* 97, 28 (1999): p. 64.
4. M. Thammachart, Y. Gunaltun, S. Punpruk, "The Use of Inspection Results for the Evaluation of Batch Treatment Efficiency and the Remaining Life of the Pipelines Subjected to Top of Line Corrosion," CORROSION/2008, paper no. 8471 (Houston, TX: NACE, 2008).
5. Y. Gunaltun, D. Larrey, "Correlation of Cases of Top of the Line Corrosion with Calculated Water Condensation Rates," CORROSION/2000, paper no. 71 (Houston, TX: NACE, 2000).
6. J.R. Piccardino, M. Stuvik, Y. Gunaltun, T. Pornthep, "Internal Inspection of Wet Gas Line Subject to Top of Line Corrosion," CORROSION/2004, paper no. 4354 (Houston, TX: NACE, 2004).
7. M. Edwards, B. Cramer, "Top of the Line Corrosion—Diagnostic, Root Cause Analysis And Treatment," CORROSION/2000, paper no. 72 (Houston, TX: NACE, 2000).
8. D.F. Ho-Chung-Qui, A.I. Williamson, P. Eng, "Corrosion Experiences and Inhibition Practices in Wet Sour Gathering Systems," CORROSION/1987, paper no. 46 (Houston, TX: NACE, 1987).
9. S. Olsen, A. Dugstad, "Corrosion Under Dewing Conditions," CORROSION/2003, paper no. 3472 (Houston, TX: NACE, 2003).
10. C. DeWaard, U. Lotz, D.E. Milliams, *Corrosion* 47, 12 (1991): p. 976-985.
11. Y. Gunaltun, R. Piccardino, D. Vinazza, "Interpretation of MFL and UT Inspection Results in Case of Top of Line Corrosion," CORROSION/2006, paper no. 6170 (Houston, TX: NACE, 2006).
12. B.F.M. Pots, E.L.J.A. Hendriksen, "CO<sub>2</sub> Corrosion Under Scaling Conditions—The Special Case of Top-of-the-Line Corrosion in Wet Gas Pipelines," CORROSION/2000, paper no. 31 (Houston, TX: NACE, 2000).
13. F. Vitse, Y. Gunaltun, D. Larrey de Torreben, P. Duchet-Suchaux, *Corrosion* 59, 12 (2003): p. 1075-1084.
14. F. Vitse, K. Alam, Y. Gunaltun, D. Larrey de Torreben, and P. Duchet-Suchaux, "Semi-Empirical Model for Prediction of the Top-of-the-Line Corrosion Risk," CORROSION/2002, paper no. 2245 (Houston, TX: NACE, 2002).
15. F. Vitse, "Experimental and Theoretical Study of the Phenomena of Corrosion by Carbon Dioxide Under Dewing Conditions at the Top of a Horizontal Pipeline in Presence of a Non-Condensable Gas" (Ph.D. diss., Russ College of Engineering, Department of Chemical Engineering, Ohio University, Athens, OH, 2002).
16. M. Singer, S. Nešić, Y. Gunaltun, "Top of the Line Corrosion in Presence of Acetic Acid and Carbon Dioxide," CORROSION/2004, paper no. 4377 (Houston, TX: NACE, 2004).
17. C. Mendez, M. Singer, A. Camacho, S. Hernandez, S. Nešić, "Effect of Acetic Acid, pH and MEG on CO<sub>2</sub> Top of the Line Corrosion," CORROSION/2005, paper no. 5278 (Houston, TX: NACE, 2005).
18. J.L. Crolet, M. Bonis, "The Role of Acetate Ions in CO<sub>2</sub> Corrosion of Carbon Steel," CORROSION/1983, paper no. 160 (Houston, TX: NACE, 1983).
19. A.M.K. Halvorsen, T. Andersen, E. Halvorsen, G. Kojen, J. Skar, "The Relationship Between Internal Corrosion Control Method, Scale Formation, and MEG Handling of a Multiphase Carbon Steel Carrying Wet Gas with CO<sub>2</sub> and Acetic Acid," CORROSION/2007, paper no. 7313 (Houston, TX: NACE, 2007).
20. T. Andersen, A.M.K. Halvorsen, A. Valle, G. Kojen, "The Influence of Condensation Rate and Acetic Acid Concentration on TOL Corrosion in Multiphase Pipelines," CORROSION/2007, paper no. 7312 (Houston, TX: NACE, 2007).
21. R. Nyborg, A. Dugstad, "Top of the Line Corrosion and Water Condensation Rates in Wet Gas Pipelines," CORROSION/2007, paper no. 7555 (Houston, TX: NACE, 2007).
22. Z. Zhang, D. Hinkson, M. Singer, H. Wang, S. Nešić, *Corrosion* 63, 11 (2007): p. 1051-1062.
23. A. Camacho, M. Singer, B. Brown, S. Nešić, "Top of the Line Corrosion in H<sub>2</sub>S/CO<sub>2</sub> Environments," CORROSION/2008, paper no. 8470 (Houston, TX: NACE, 2008).
24. M. Singer, A. Camacho, B. Brown, S. Nešić, *Corrosion* 67, 8 (2011): p. 085033.
25. D. Hinkson, M. Singer, Z. Zhang, S. Nešić, *Corrosion* 66, 6 (2010): p. 045002.
26. E. Remita, B. Tribollet, B. Sutter, F. Ropital, X. Longaygue, J. Kittel, C. Taravel-Condât, N. Desamais, *J. Electrochem. Soc.* 155, 1 (2008): p. C41-C45.
27. J. Amri, E. Gulbrandsen, R.P. Nogueira, *Electrochem. Comm.* 10 (2008): p. 200-203.
28. M. Singer, B. Brown, A. Camacho, S. Nešić, *Corrosion* 67, 1 (2011): p. 015004.
29. ASTM G1-03, "Standard Practice for Preparing, Cleaning, and Evaluating Corrosion Test Specimens" (West Conshohocken, PA: ASTM International, 2009), p. 17-23.